Chapter 7

Stepwise Hydration of the Sulfate Dianion

7.1 Doubly Charged Anions

Chemists view most ionic crystals as composed of *autonomously stable* negative and positive ions [232]. These building block ions can be singly or multiply charged (e.g. NaCl consists of Na^+ and Cl^- ions, and $MgSO_4$ contains Mg^{2+} and SO_4^{2-} ions), but they are expected to be stable to the extent that they can be characterized in the laboratory. Dividing crystals, melts, and ionic molecules into positive and negative ions is usually performed via the octet rule. For example, K_2SO_4 salt is considered to be composed of K^+ cations and SO_4^{2-} anions, within which all constituent atoms posses full octets of valence electrons. Within this point of view, chemists interpret the physical, reactive, optical, and other properties of crystals, melts, and liquid ionic salts in terms of properties intrinsic to the corresponding positive and negative ions. For example, in NH_4Cl, one interprets Raman spectra in terms of crystal phonons as well as internal $N\!-\!H$ vibrations belonging to the NH_4^+ cation.

This widely accepted approach in chemistry is called into question when one recognizes that many multiply charged anions that occur frequently in salts do not necessarily exist as autonomously stable species in which the extra electrons occupy valence molecular orbitals. How can one view the composition of a ionic material such as a salt in terms of building blocks that cannot be isolated and thus fully characterized [232]? Until about fifteen years ago, no experimental evidence had been found for the existence of multiply charged anions [233].

When discussing the stability of multiply charged anions, three types of stability are considered. The first is electronic stability of the anion. If A^{n-}, at its own optimal geometry, is more stable than the corresponding $A^{(n-1)-}$ at the same geometry, A^{n-} is said to be *vertically electronically stable*. If A^{n-} at its optimal geometry is more

stable than $A^{(n-1)-}$ at its own optimal geometry, A^{n-} is said to be *adiabatically electronically stable*. In addition, there is the issue of geometrical stability. If A^{n-} has all real vibrational frequencies at its optimal geometry, it is *locally geometrically stable*. Finally, if A^{n-} is more stable than any possible dissociation fragment, it is *thermodynamically stable*. Clearly, if an anion is thermodynamically stable, it must also be electronically and geometrically stable.

Most small multiply charged anions are not thermodynamically stable, although most are electronically and locally geometrically stable and may have large barriers to dissociation or to autodetachment. Such anions can be studied experimentally because they are long-lived.
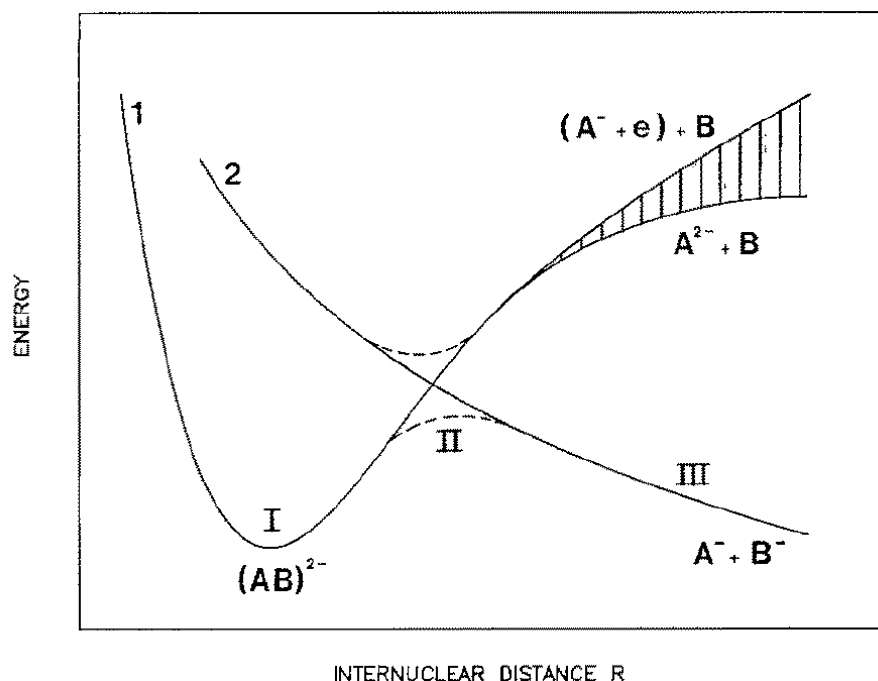

Figure 7.1: Schematic drawing of potential energy curves illustrating the intersection of two adiabatic states (solid lines): a state supporting vibrations (curve 1) and a repulsive state (curve 2). The former state correlates asymptotically with A^{2-}+B if A^{2-} exists and otherwise with a short-lived resonance $(A^-+e)+B$. The shaded area indicates a possible "broadening" due to the finite lifetime of the resonance state. The repulsive state correlates asymptotically with A^-+B^-. The avoided crossing between the corresponding adiabatic curves is indicated by the broken lines. From Reference [233].

The concept of a doubly negative molecule interacting along a Coulombic repulsive surface as two singly negative species seems to exclude any possibility of stable states. However, at some distances, chemical forces can lead to a local minimum in the

potential energy surface behind a Coulombic barrier. If the minimum is sufficiently deep to support the zero point vibrations, one may encounter a metastable dianion. See Figure 7.1.

For a dianion $(AB)^{2-}$ one supposes an attractive state correlating with either a A^{2-}+B asymptote or with $(A^{-}+e)$+B (curve 1) according to whether or not a constituent A of the molecule can support two additional electrons. The other state (curve 2) is strongly repulsive being essentially Coulombic in character and correlates with A^{-}+B^{-}. Asymptotically this curve falls off as $1/R$, where R is the distance between the centers of charge in A^{-} and B^{-}. The resulting adiabatic potential energy surface exhibiting a local maximum is thought to arise from an avoided crossing between these two states.

As is shown in Figure 7.1, one expects three main features characterizing the potential energy surface: a local minimum (I) reflecting the most stable conformation of the dianion, a local maximum (II) at somewhat larger inter-nuclear distance and finally a repulsive part (III) at large distances mainly dominated by the $1/R$ potential between the two charged fragments. If the height and/or width of the barrier are large, a free dianionic molecule can be stable to dissociation [233].

Another interesting perspective on multiply charged anions (MCA) is their behavior upon photoionization [234]. Photoionization of a neutral molecule produces a positive ion and an outgoing electron (Figure 7.2a); photodetachment of a singly charged molecular anion also produces an outgoing electron and a neutral molecule (Figure 7.2b). In both cases, the long-range interactions between the photo-products are attractive in nature. However, photodetachment of a MCA results in two negatively charged (a free electron and a negative ion with one less charge than the parent MCA), whose long-range interactions are mainly the Coulomb repulsion (Figure 7.2c). As discussed above, the superposition of the short-range binding of the electron and the long-range Coulomb repulsion give rise to a potential barrier for the outgoing electron. This repulsive Coulomb barrier (RCB) leads to interesting phenomena in photodetachment experiments. For example, Wigner's threshold law[1] [235] of photodetachment would not hold and threshold photodetachment of MCAs is simply not feasible. Thus one has the interesting situation, where, if the detachment photon energy is below the RCB, no electron detachment will occur even if the photon energy is above the asymptotic electron binding energy (see Figure 7.2d). In this case, detachment can only take place through electron tunneling, which at threshold would have negligible probability. Therefore, photoelectron spectroscopy experiments can only be accomplished by using photon energies higher than the RCB [236, 237].

Even more interesting is the case where the long-range Coulomb repulsion is

---

[1]"The cross section is, apart from a constant, in the neighborhood of the threshold the same function of energy, no matter what the reaction mechanism is, as long as the long-range interaction of the product particles is the same" [235].
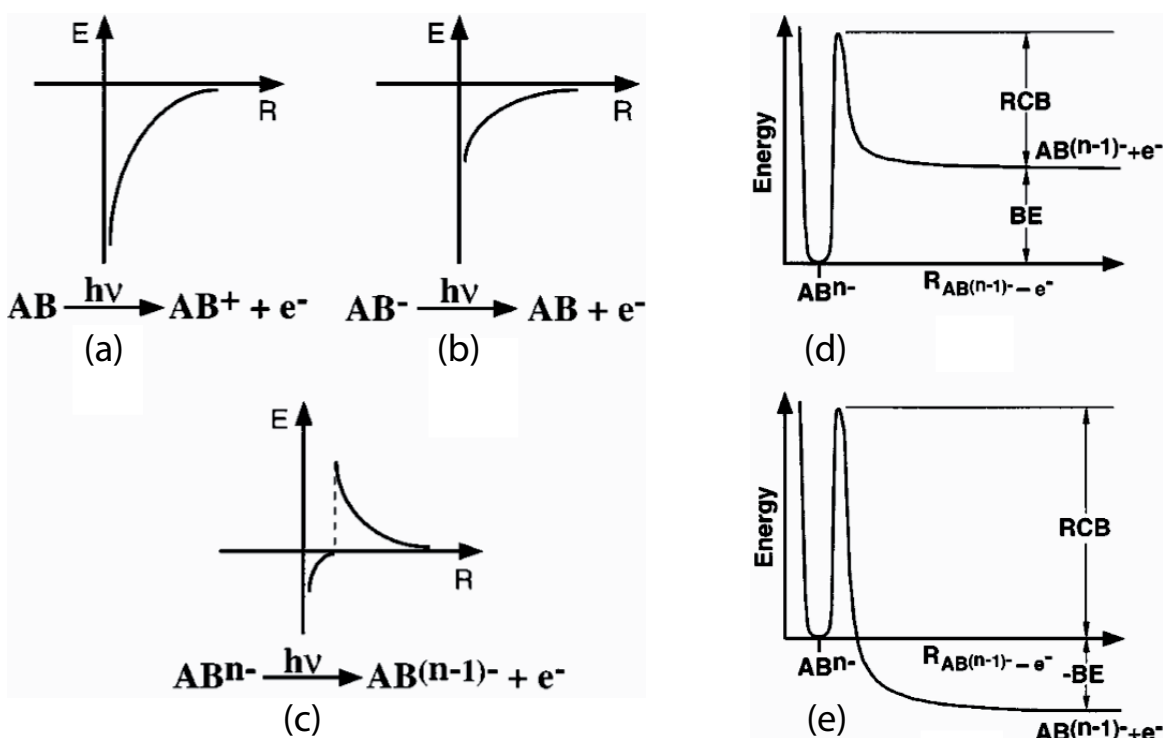
Figure 7.2: Schematic potential energy curves for (a) photoionization of a neutral molecule, (b) photodetachment of a singly charged anion, and (c) photodetachment of a multiply charged anion. On the right side, schematic potential energy curves showing the excess electron binding energy (BE) and the repulsive Coulomb barrier (RCB) in multiply charged anions: (d) for an electronically stable multiply charged anion with a positive BE; (e) for an electronically unstable multiply charged anion with a negative BE [234].

stronger than the short-range electron binding, resulting in metastable MCAs (Figure 7.2e). In this case, the $AB^{(n-1)-}$ anion is electronically more stable than the AB^{n-} MCA, which thus possesses a negative electron binding energy (Figure 7.2e). This would result in an unusual phenomenon in photoelectron spectroscopy experiments that the outgoing electron kinetic energy would be higher than the incoming photon energy. The extra energy derives from the electrostatic energy stored in the AB^{n-} MCA [238, 239].

Until very recently, small molecular MCA have predominately been a matter of theoretical studies [233, 240]. The limited number of experimental reports can primarily be attributed to the lack of appropriate experimental methods to generate small or medium-sized MCA. For example, while (dissociative) electron ionization is well-suited to generate multiply charged cations as well as monoanions, in the case of dianions there exists a fundamental conflict between generating reactive species

having reasonably high electron affinities on one hand and the hyperthermal nature of the ionization method on the other hand [240].

A solution of this experimental dilemma has been provided by electrospray ionization. A priori, the electrospray approach is only limited as far as highly reactive species are concerned because the ions emanate from solution, thereby only allowing generation of ions which do not react with the solvent(s) present.

7.2   The Sulfate Dianion

Multiply-charged anions (MCAs) and their hydrates are fundamental to condensed phase chemistry and biology in very diverse environments. For example, hydrated sulfate dianions play a key role in the homogeneous nucleation of ice particles by sulfate aerosols in the upper troposphere [241], activity lowering in fuel cells by adsorbed sulfate ions on platinum-based electrodes [242], and regulation of many metabolic and cellular processes [243].

While penta-atomic dianions of the form MF_4^{2-} (e.g., BeF_4^{2-}, MgF_4^{2-}, CaF_4^{2-}) are predicted to be stable to loss of an extra electron but to be thermodynamically unstable to loss of F^- [233, 244], the isoelectronic oxide dianion SO_4^{2-} does not support two electrons [245–247].

In solution and crystalline phases, sulfate ions are stabilized through electrostatic interactions with solvent molecules and counterions. In the gas phase, similar stabilization can be achieved by hydration, and both experiment and theory agree that a minimum of three water molecules are needed to stabilize the SO_4^{2-} dianion against spontaneous electron loss [247, 248].
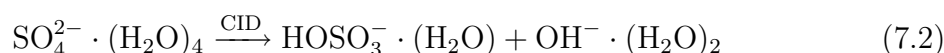
A microscopic, molecular level understanding of the role of hydrated sulfates in chemical and biological relevant processes requires elucidation of the solute-solvent interactions and the precise arrangement of the water molecules comprising the solvation shell [249]. In particular, one would like to probe in detail how the solvent network evolves in a step-wise manner around the dianionic core, providing the opportunity to study novel hydrogen-bonding motifs differing from those seen in the hydration of singly-charged anions.

Hydrated sulfate $SO_4^{2-} \cdot (H_2O)_n$ clusters were first observed in the gas phase by Blades and Kebarle [247]. They observed that the smallest number of water molecule to stabilize the sulfate dianion in the gas phase is n=3, although they were able to detect small quantities of $SO_4^{2-} \cdot (H_2O)_2$ after collision induced dissociation of the $SO_4^{2-} \cdot (H_2O)_4$ cluster. Collision products need to be stable for a few microseconds in order to be detected. Blades and Kebarle observed the peak corresponding to $SO_4^{2-} \cdot (H_2O)_{12}$ in the mass spectrum to be the most intense. They investigated the fragmentation channels of the hydrate sulfate by collision induced dissociation (CID) and they found two main dissociation patterns. For larger values of n (e.g. $n=14$) the

dominant dissociation channel is water loss:

$$\mathrm{SO_4^{2-}} \cdot \mathrm{(H_2O)}_n \xrightarrow{\mathrm{CID}} \mathrm{SO_4^{2-}} \cdot \mathrm{(H_2O)}_k + \mathrm{(H_2O)}_{n-k} \tag{7.1}$$
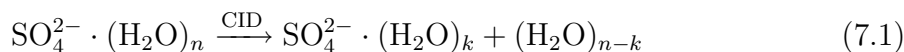
They had evidence that equation (7.1) proceeds predominantly by consecutive water losses and they observed that the maximum in the fragments mass spectrum was at $n=7$, where the consecutive ligand loss begins to slow down. They suggested that an inner solvation shell closes at $n=7$. On the basis of the CID conditions they estimated the water to ion bond energies to be $\sim$15 kcal/mol (0.65 eV) for the species in the range n=8–14. For smaller values of n (e.g. $n=4$), charge separation becomes the dominant channel:

$$\mathrm{SO_4^{2-}} \cdot \mathrm{(H_2O)}_4 \xrightarrow{\mathrm{CID}} \mathrm{HOSO_3^-} \cdot \mathrm{(H_2O)} + \mathrm{OH^-} \cdot \mathrm{(H_2O)}_2 \tag{7.2}$$

This reaction can be viewed as intramolecular proton transfer from HOH to $\mathrm{SO_4^{2-}}$. In solution these reactions are strongly endoergic, i.e., $\mathrm{HSO_{4(aq)}^-}$ is a very much stronger acid than HOH, but the Coulombic repulsion in the cluster, which increases rapidly as the number of water molecules is decreased, makes the proton transfer become less endoergic than the $\mathrm{H_2O}$ ligand loss.

The first spectroscopic studies on $\mathrm{SO_4^{2-}} \cdot \mathrm{(H_2O)}_n$ clusters were performed by Wang and coworkers [248, 249] whose photoelectron (PE) spectra provided an estimate of the repulsive Coulomb barrier and the stepwise hydration energies. Blackbody infrared radiative dissociation experiments [250] measured water loss rates for clusters with $n=3$–17, finding that the $n=6$ and $n=12$ complexes are particularly stable. Several groups [248, 250–254] have investigated these clusters using electronic structure and molecular dynamics calculations, finding that the dianion is internally solvated, in contrast with observations for many singly-charged anions [255]. However, the computational studies obtained multiple structural isomers for each cluster size, with varying degrees of water-water and water-sulfate hydrogen bonding, and the energetic orderings of the isomers for a given cluster size changed with the level of theory. Clearly, a direct experimental probe of the structure of these hydrated clusters is warranted.

This problem is approached here by investigating the vibrational spectroscopy of size-selected clusters in which an MCA is solvated by a known number of water molecules; this is the first such experiment on an MCA. Gas phase infrared (IR) spectra of mass-selected $\mathrm{SO_4^{2-}} \cdot \mathrm{(H2O)}_n$ dianions ($n=3$–24) are measured in the range from 540 to 1850 cm^{-1}, the spectral region containing the stretching and bending modes of the sulfate core as well as characteristic intra- and intermolecular water modes.

7.3   Experimental Details

The $\mathrm{SO_4^{2-}} \cdot \mathrm{(H_2O)}_n$ clusters are produced from electrospray (see section 2.1) of a 10^{-3} M tetra-butylammonium sulfate solution in water/acetonitrile mixed solvent (15/85 vol-

ume ratio) at neutral pH. This is the same solution used by Wang and coworkers in their photoelectron spectroscopy studies [256]. A typical mass spectrum is shown in Figure 7.3. By adjusting the electrospray source conditions it is possible to shift the center of the hydrated sulfate dianion clusters distribution (see Figure 7.4). Clusters with up to 60 water molecules can be produced. The smallest cluster that can be observed is $SO_4^{2-} \cdot (H_2O)_3$. The dominant mass peak is HSO_4^- (off scale in Figure 7.3). Together with the $SO_4^{2-} \cdot (H_2O)_n$ series, the $HSO_4^- \cdot (H_2O)_n$ and the $HCO_2^- \cdot (H_2O)_n$ series are observed. The identity and origin of the last series is due to the presence of carbonate impurities in the tetra-butylammonium sulfate solution.

FELIX is coupled to the machine using the KRS5-setup (see Section 2.2). In the present experiments, the FELIX bandwidth is about 0.2% of the central wavelength and the pulse energy is 10–40 mJ per macropulse, measured before the KRS5 and KBr optics. The dissociation energies required for various cluster sizes differ [257]; approximately, 3 to 10 photons are needed for dissociation in the frequency range studied here. However, some of the parent ions dissociate upon trapping due to collisions with the buffer gas. These fragment ions also absorb IR radiation and further dissociate, complicating the interpretation of the daughter ion spectra. Therefore all IR-PD spectra are measured by monitoring the depletion of the parent ion. For each cluster size, overview spectra are first acquired to pinpoint the bands, and then each band is scanned with the required FEL attenuation to avoid saturation of the absorption. Figure 7.5 shows only the attenuated composite spectra.

7.4   Results

IR-PD spectra for the various clusters are displayed in Figure 7.5. There are four bands that appear prominently in the spectra, labeled A–D in the figure. Based on comparison with known features of the IR-spectra of the constituents of the clusters, these features are assigned as follows. In solution, the tetrahedrally symmetric sulfate dianion shows two modes in the spectral region of this study: the antisymmetric stretching (ν_3) and bending (ν_4) modes at 1106 and 617 cm^{-1}, respectively [258]. These modes are assigned to the bands labeled B and D in Figure 7.5, which fall in the ranges 1080–1110 cm^{-1} and 615–626 cm^{-1}, respectively. The IR spectrum of liquid water also exhibits two bands in this spectral region: the intramolecular bending mode at 1645 cm^{-1}, [259] and the intermolecular frustrated rotation, or librational mode, at 683 cm^{-1} [260]. Accordingly, these modes are assigned to bands A and C, which occur between 1735–1674 and 864–681 cm^{-1}, respectively, in the IR-PD spectra. Several weaker bands appear in the spectra of the smallest clusters (indicated with asterisks in Figure 7.5), they are tentatively assigned to combination bands, consistent with unpublished results calculated by Gerber and Miller [261]. Possibly, these combination bands are found only for the smaller clusters that are more strongly bound and thus
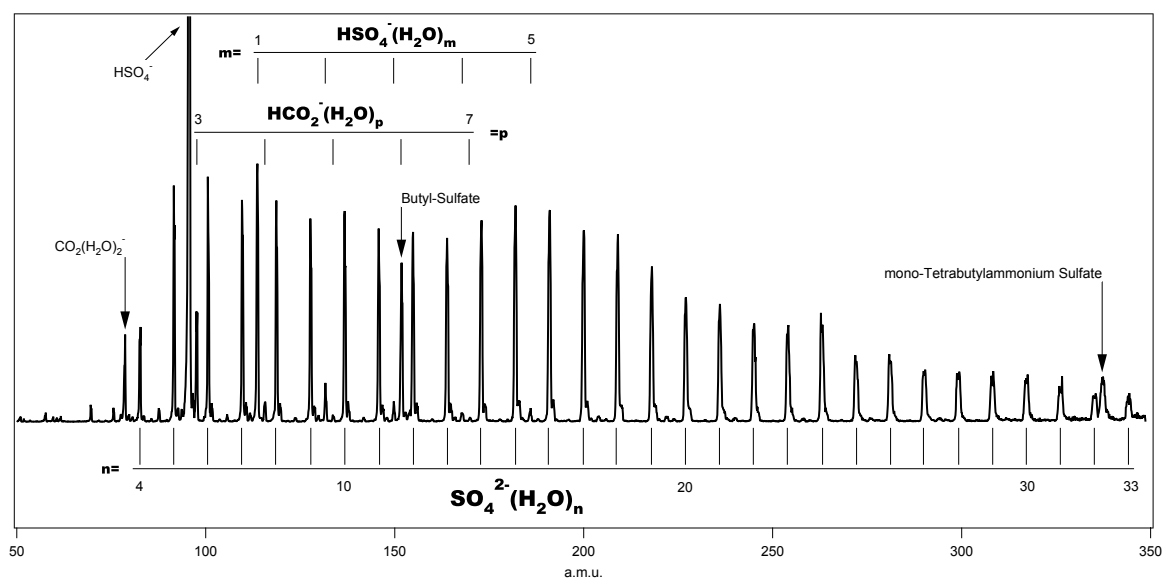
Figure 7.3: A typical mass spectrum of the ions produced by electrospray of a 10^{-3} M tetra-butylammonium sulfate solution in water/acetonitrile (15/85 volume ratio) mixed solvent at neutral pH. The series of the hydrated sulfate $SO_4^{2-} \cdot (H_2O)_n$ dianions can be distinguished for $n=4$–33.
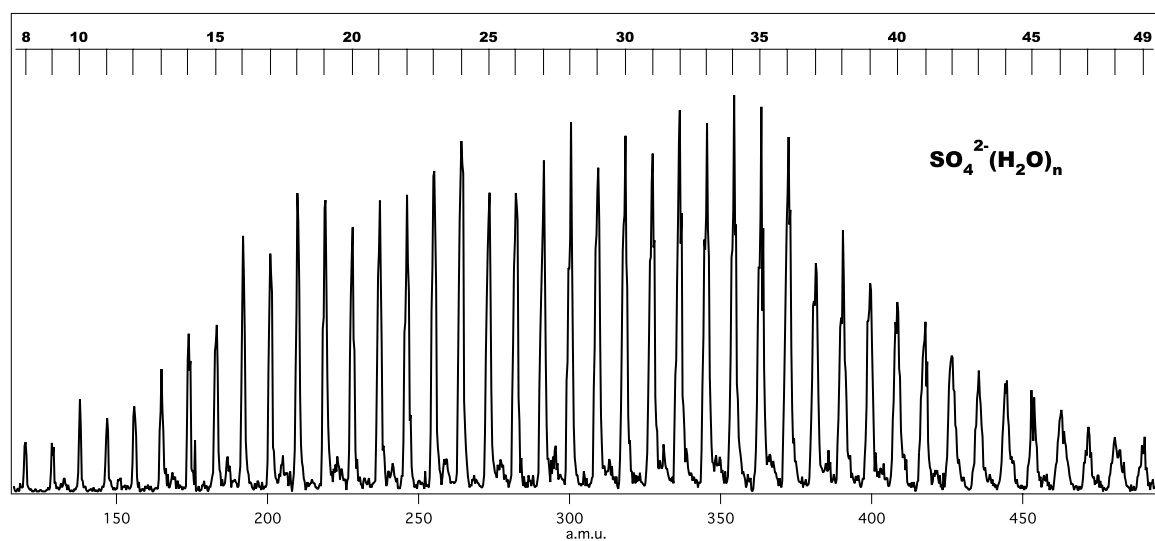

Figure 7.4: By adjusting the electrospray ion source conditions, hydrated sulfate dianion clusters with up to 60 water molecules are produced. Here a mass spectrum is shown for $SO_4^{2-} \cdot (H_2O)_n$ with $n=8$–49

necessitate higher FELIX fluences to achieve photodissociation. Extra features in the spectra of $n=13$ and 14 clusters are found to arise from changes in the hydration

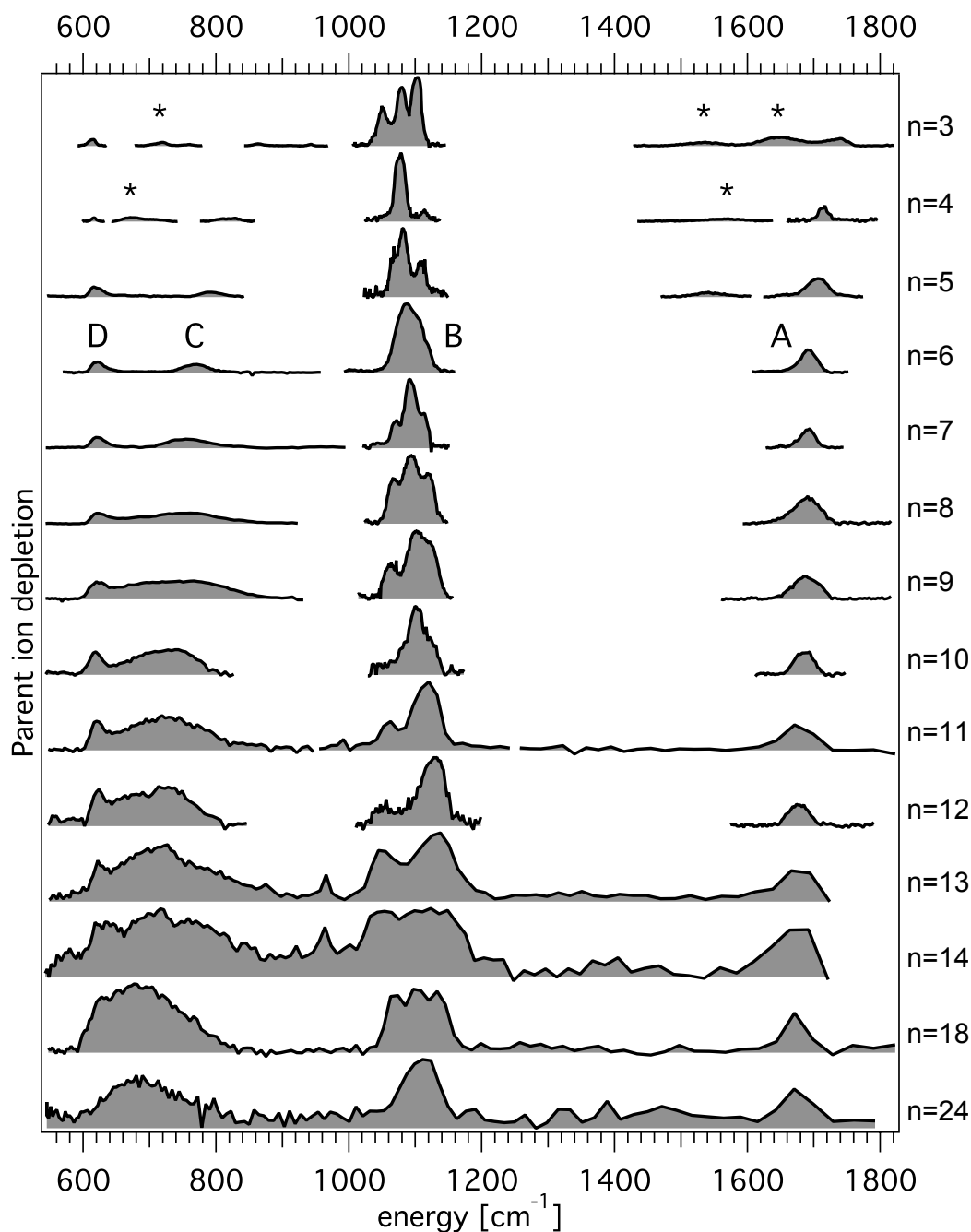structure around the sulfate as discussed below.

Figure 7.5: Experimental spectra of $SO_4^{2-} \cdot (H_2O)_n$ with n=3–14, 18, and 24. Bands A–D (indicated in the n=6 spectrum) are assigned as described in the text. Peaks indicated with an asterisk (*) are tentatively assigned to combination bands.

The size-dependent trends observed for the experimental spectra provide further support for the assignments given above. For example, the water bands A and C are initially quite weak compared to the sulfate band B, but grow with increasing cluster size. In addition, the band positions start out perturbed from the condensed phase vibrational origins, and then shift toward them gradually with increasing cluster size. The other notable size-dependent effect is the evolving shape of band B, which is, for example, a triplet in the n=3, 7, and 8 clusters, a doublet in n=5 and 9, and a singlet for n=4 and 6. The ν_3 mode assigned to this band is triply degenerate for a free sulfate ion with T_d symmetry, so the shape of this band provides a sensitive probe of the local solvent environment. The width of the librational band C increases markedly above n=6, practically doubling from n=6 to 7.

Further elucidation of the hydration configurations responsible for the experimental spectra requires comparison with electronic structure calculations. Jia Zhou and Dave T. Moore from the University of California, Berkeley, performed electronic structure calculations with GAUSSIAN [262] to obtain vibrational spectra and optimized structures for selected clusters [263]. For the smaller (n=3–7) clusters, calculations were carried out at both the MP2 and DFT/B3LYP levels of theory, while only DFT was used for the larger n=12 and n=13 clusters. The TZVP+ basis set was the same one used by Wang et al. [248] All structures reported represent stable minima with no imaginary frequencies. All relative energy comparisons refer to total energies that have been corrected for zero-point vibrational energy, but not for basis-set superposition error.

Figure 7.6 compares calculated (MP2/TZVP+) and experimental spectra for the smaller clusters (n=3–6), along with images of the lowest energy cluster structures. The splitting pattern of band B provides a key point of comparison. The calculated spectra show that band B is quite strongly split for the low-symmetry C_2 n=3 structure, where the solvation of the sulfate O-atoms is anisotropic. This splitting disappears for the isotropically solvated and highly symmetric D_{2d} n=4 and T_d n=6 structures, where each of the sulfate O-atoms accept 2 and 3 hydrogen bonds, respectively. The C_{2v}-symmetry n=5 structure is an intermediate case, exhibiting a smaller splitting than n=3, corresponding to a less anisotropic solvation environment. For all cases in Figure 7.6, the calculated and experimental splitting patterns of band B are in reasonable agreement.

The water ligands in all of the structures in Figure 7.6 exhibit the same "bridging" H-bonding motif, where each water acts as a double-donor to two sulfate O-atoms. This result differs from other computational studies using DFT and/or smaller basis-sets, in which the lowest-energy structures included a mixture of bridging waters and waters with one sulfate and one water-water H-bond [248, 252–254]. For n=3–6, the mixed structures have, in general, slightly higher energies (including zero-point vibrational correction) at the MP2/TZVP+ level of theory, and that their calculated spectra yield a poorer match with experiment. For example, Figure 7.7(left) compares
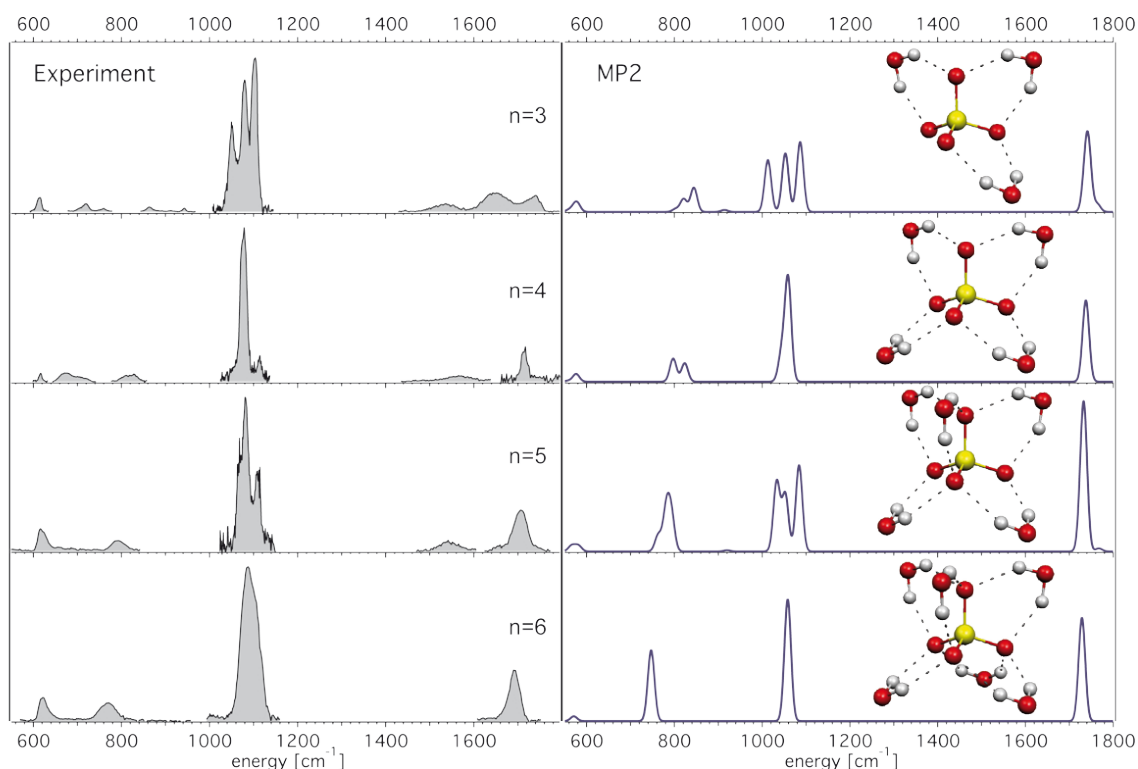
Figure 7.6: Experimental vs calculated spectra for small hydrated sulfate clusters (n=3–6). Calculated (MP2) spectra for the lowest energy isomers of the n=3–6 clusters are shown in the right-hand column (15 cm^{-1} FWHM Gaussian convolution), along with pictures of the calculated cluster structures.

the structures and spectra for two isomers of SO$_4^{2-}$·(H$_2$O)$_6$: the T_d structure mentioned above, and a C_3 symmetry isomer where 3 of the water ligands form a cyclic trimer unit. The water-water H-bonds in the latter structure give rise to an extra band at 865 cm^{-1} in the calculated spectrum that is clearly absent from the experimental spectrum.

The structures in Figure 7.6 imply that the driving force stabilizing these smaller clusters is solvation of the negatively-charged sulfate O-atoms through hydrogen bonding. Following this trend, a seventh water cannot bind to the sulfate solvated in the n=6 cluster without causing rearrangement of the initial six ligands. Figure 7.7(right) compares the calculated spectra for such a "rearranged" isomer to a "6+1" isomer where the n=6 T_d core is retained, and the additional water is added to an outer shell. The latter isomer gives a better overall match to the IR-PD spectrum, particularly in the position of the intermolecular librational band that is expected to be most sensitive to H-bond rearrangements. However, the two calculated spectra are not sufficiently distinct to rule out the presence of the rearranged isomer, so it may be that both
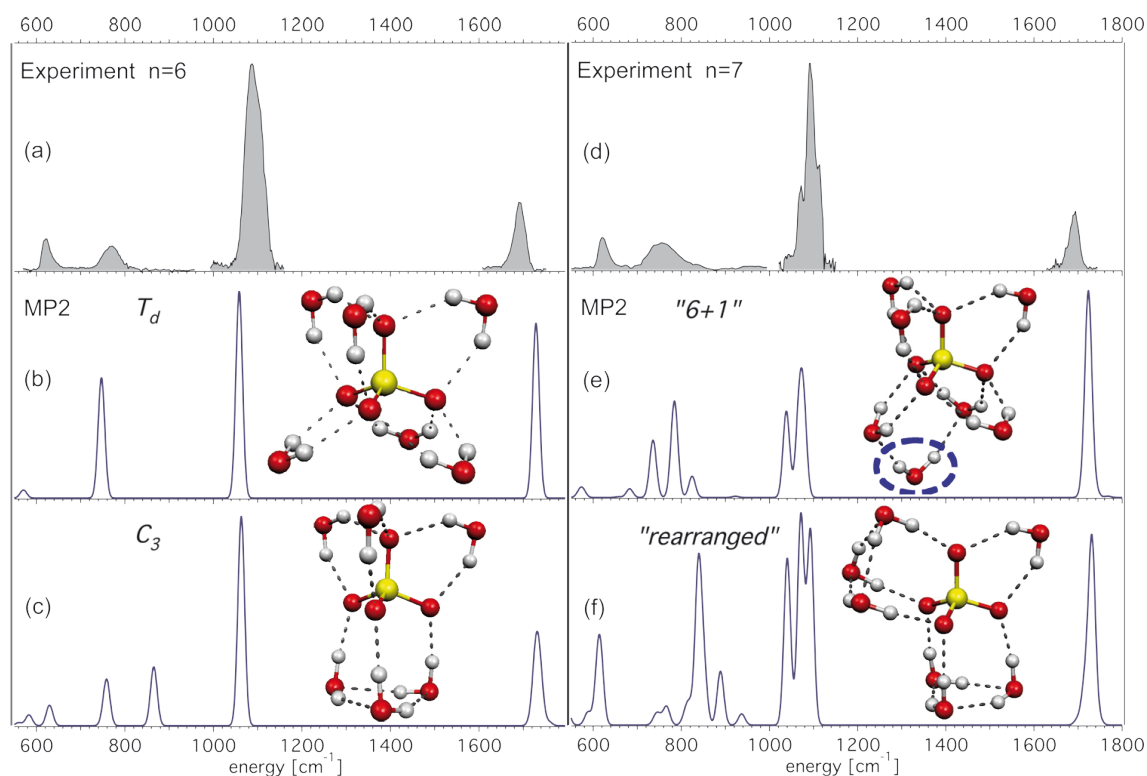
Figure 7.7: (a) Experimental spectrum for $SO_4^{2-}\cdot(H_2O)_6$. Calculated spectrum and structure for T_d, (b), and C_3, (b), isomers of $SO_4^{2-}\cdot(H_2O)_6$. The computed relative energies indicate that these $n=6$ isomers are essentially isoenergetic, with B3LYP favoring the C_3 isomer by ∼5 kJ/mol, and MP2 favoring the T_d isomer by ∼1 kJ/mol. (d) Experimental spectrum for $SO_4^{2-}\cdot(H_2O)_7$. Calculated spectrum and structure for the "6+1", (e), and "rearranged", (f), isomers of $n=7$ (see text). The dashed circle indicates the "outer shell" water in the "6+1" structure. Similar to $n=6$, the computed relative energies indicate these $n=7$ isomers are essentially isoenergetic, with both B3LYP and MP2 favoring the rearranged isomer by ∼5 kJ/mol and ∼0.1 kJ/mol, respectively. All of the other H-bonding motifs involving water-water H-bonds produced $n=6$ and $n=7$ structural isomers that were significantly higher in energy.

isomers are represented in the IR-PD spectrum. For both $n=6$ and 7, the computed energies of two isomers are the same within the (estimated) uncertainty.

Figure 7.8 compares experimental and calculated spectra for the $n=12$ and $n=13$ clusters, along with the lowest energy calculated structures. The symmetric (T point group) $n=12$ structure is similar to those reported previously [252, 254], and gives reasonable agreement with the experimental spectrum. In reference to the above discussion of the driving forces determining H-bonding, this structure maximizes cluster
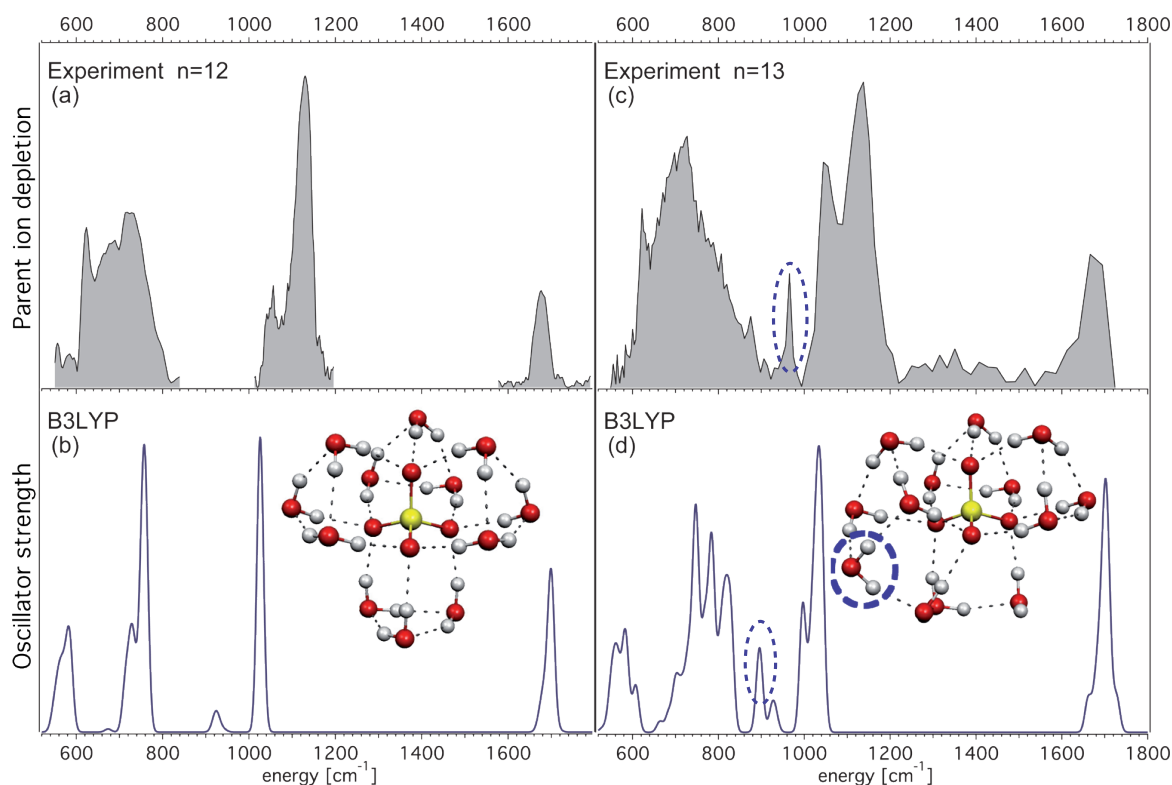
Figure 7.8: Experimental vs calculated spectra for large hydrated sulfate clusters (n=12, 13). Calculated spectra (B3LYP) for the lowest energy isomer of the n=12, 13 clusters are shown on the bottom, (b) and (d), (15 cm^{-1} FWHM Gaussian convolution), along with pictures of the calculated cluster structures. The corresponding experimental spectra are shown above for comparison. The dashed circles for n=13 indicate the water in the second solvation shell, along with the associated vibrational bands in the calculated and experimental spectra. The B3LYP frequencies are not scaled. Comparative calculations for the smaller clusters have shown that B3LYP systematically underestimates the sulfate antisymmetric stretch frequencies by $\sim$80 cm^{-1}, compared to the experimental data. However, both B3LYP and MP2 reproduced the positions of the water bands quite well.

stabilization by having each sulfate O-atom solvated by three H-bonds, and the waters organized into four cyclic trimer moieties, one for each face of the sulfate tetrahedron. The experimental n=13 spectrum contains a new peak near 950 cm^{-1}, an otherwise inactive region in the spectra. It also shows a broadening of the librational band (band C) on the high-wave number side, and a shoulder on the low-wave number side of the sulfate stretching band (band B). The calculated spectrum exhibits similar features, most notably the peak in the 900 cm^{-1} region that is not present in the n=12 spectrum. Examination of the calculated vibrational normal modes indicates

that this mode is localized on the 13th water molecule, which resides outside the first solvation shell (dashed circle in Figure 7.8). The appearance of this peak in both the experimental and calculated spectra provides strong indication that the 13th water does indeed go on the second solvation shell.

A picture of the sequential solvation of the sulfate dianion arises from the above discussion. For the smaller sizes (n=3–6), each water adds to an open edge of the sulfate tetrahedron in a "bridging" fashion, forming H-bonds to adjacent sulfate O-atoms. This solvation structure can incorporate a maximum of six bridging waters. Above n=6, formation of water-water H-bonds becomes competitive with bridging ligands. This trend is made apparent by the broadening of the librational band for n$\geq$7 and from comparison with theory (Figure 7.7). The exact nature of the water solvation shell for n=7 cannot be determined, since there is no single spectroscopic feature that allows one to choose between the two calculated structures in Figure 7.7. On the other hand, shell-closure at n=12 is indicated experimentally by the appearance of a new band in the spectra of the n=13 and n=14 clusters, associated with the libration of water molecules in the second solvation shell. Interestingly, these bands are not present in the n=18 and in the n=24 spectra, suggesting that a change in arrangement must arise for those larger clusters.

These results are the first infrared spectra of a solvated MCAs in the gas phase. They provide new insights into the structure of these complexes. Overall, from the observed vibrational frequencies of both the dianion and the solvent, the complexes can be seen as a distorted tetrahedral SO$_4^{2-}$ core surrounded by H$_2$O molecules. No evidence for low-frequency ($\sim$1000 cm^{-1}) stretch and bend frequencies associated with a shared proton is observed, in contrast to singly-charged cations and anions with strong hydrogen bonds such as H$_5$O$_2^+$ and H$_3$O$_2^-$ [231, 264]. The absence of such features reflects the delocalization of negative charge in the sulfate ion over the four oxygen atoms, so that the individual hydrogen bonds with the surrounding water molecules are weaker than in singly-charged species with strong H-bonds.